OPEN

Molecular profiling of Spitz nevi identified by digital RNA counting

Lisa M. Hillen[a], Milan S. Geybels[b], Dorit Rennspiess[a], Ivelina Spassova[c], Cathrin Ritter[c], Jürgen C. Becker[c], Marjan Garmyn[e], Axel zur Hausen[a], Joost Van den Oord[d] and Véronique Winnepenninckx[a]

The molecular properties of benign melanocytic lesions are poorly understood. Only a few studies have been carried out on specific nevi subtypes, including common nevocellular nevi (NCN) or Spitz nevi (SN). Genomic alterations in melanoma-associated oncogenes are typically absent in SN. In the present study, mRNA expressions of 25 SN and 15 NCN were analyzed. Molecular profiling was performed using the RNA NanoString nCounter Gene Expression Platform (number of genes = 770). Marker discovery was performed with a training set consisting of seven SN and seven NCN samples from the same patients, and validation was performed using a second set consisting of 18 SN and eight NCN samples. Using the training set, 197 differentially expressed genes were identified in SN versus NCN. Of these, 74 genes were validated in the validation set (false discovery rate $q \leq 0.13$). In addition, using random forest and least absolute shrinkage and selection operator feature selection, a molecular signature of SN versus NCN was identified including 15 top-ranked genes. The present study identified a distinct molecular expression profile in SN compared with NCN, even when lesions were obtained from the same patients. Gene set analysis showed upregulation of gene pathways with increased expression of transcripts related to immunomodulatory, inflammatory, and extracellular matrix interactions as well as angiogenesis-associated processes in SN. These findings strongly indicate that SN represent a distinct group of melanocytic neoplasms and evolve differentially and not sequentially from NCN. *Melanoma Res* 28:510–520 Copyright © 2018 The Author(s). Published by Wolters Kluwer Health, Inc.

Melanoma Research 2018, **28**:510–520

Keywords: gene pathways, molecular signature, mRNA, nevocellular nevi, Spitz nevus

[a]Department of Pathology, GROW-School for Oncology and Developmental Biology, Maastricht University Medical Center, [b]Department of Epidemiology, GROW-School for Oncology and Developmental Biology, Maastricht University, Maastricht, The Netherlands, [c]Department for Translational Dermato-Oncology, Center for Medical Biotechnology, University Hospital Essen, Essen, Germany, [d]Leuven Belgium and Laboratory Translational Cell and Tissue Research, Department of Pathology and [e]Laboratory of Dermatology, Department of Oncology and Dermatology, University Hospitals Leuven, University of Leuven, Leuven, Belgium

Correspondence to Véronique Winnepenninckx, PhD, Maastricht University Medical Center (MUMC+), Afdeling Pathologie, PO Box 5800, 6202 AZ Maastricht, The Netherlands
Tel: +31 433 874 612; fax: +31 433 874 618;
e-mail: v.winnepenninckx@mumc.nl

Received 13 April 2018 **Accepted** 17 July 2018

Introduction

Spitz nevi (SN) are clinically and histologically distinct pigment cell lesions that commonly arise in children and adolescents, but may also occur in older individuals [1]. Spitzoid neoplasms were first described by the American pathologist Sophie Spitz in 1948 as 'juvenile melanomas' or as 'melanomas of childhood' [2]. SN are characterized by distinct histological properties. They are composed of large epitheloid and/or spindle-shaped melanocytes with large nuclei that contain vesicular chromatin and often prominent nucleoli (Fig. 1c and d [3]). Spitzoid neoplasms with marked atypia and an aggressive clinical behavior are termed spitzoid malignant melanoma (SMM).

The distinction of SN from intermediate lesions such as atypical spitzoid tumors (AST) or spitzoid tumors of unknown malignant potential (STUMP) that may recur locally or metastasize to regional lymph nodes, but not toward distant sites, may be challenging [4–6]. Molecular alterations commonly observed in melanomas are typically absent from SN and translocations that occur in SN are usually not found in melanomas [7–9].

A major obstacle in the molecular understanding of spitzoid neoplasms is the lack of basic knowledge of the molecular–genetic events that distinguish SN from common nevocellular nevi (NCN). We hypothesized that the unique features of SN, such as their cellular and nuclear characteristics as well as their stromal features, may reflect a distinct molecular differentiation profile, and that this profile may be altered in AST/STUMP and SMM and, hence, may help in the differential diagnosis in daily surgical pathology practice.

In the current study, we used the RNA NanoString nCounter Gene Expression Platform (number of genes = 770) to

Supplemental Digital Content is available for this article. Direct URL citations appear in the printed text and are provided in the HTML and PDF versions of this article on the journal's website, www.melanomaresearch.com.

0960-8931 Copyright © 2018 The Author(s). Published by Wolters Kluwer Health, Inc. DOI: 10.1097/CMR.0000000000000495

Fig. 1

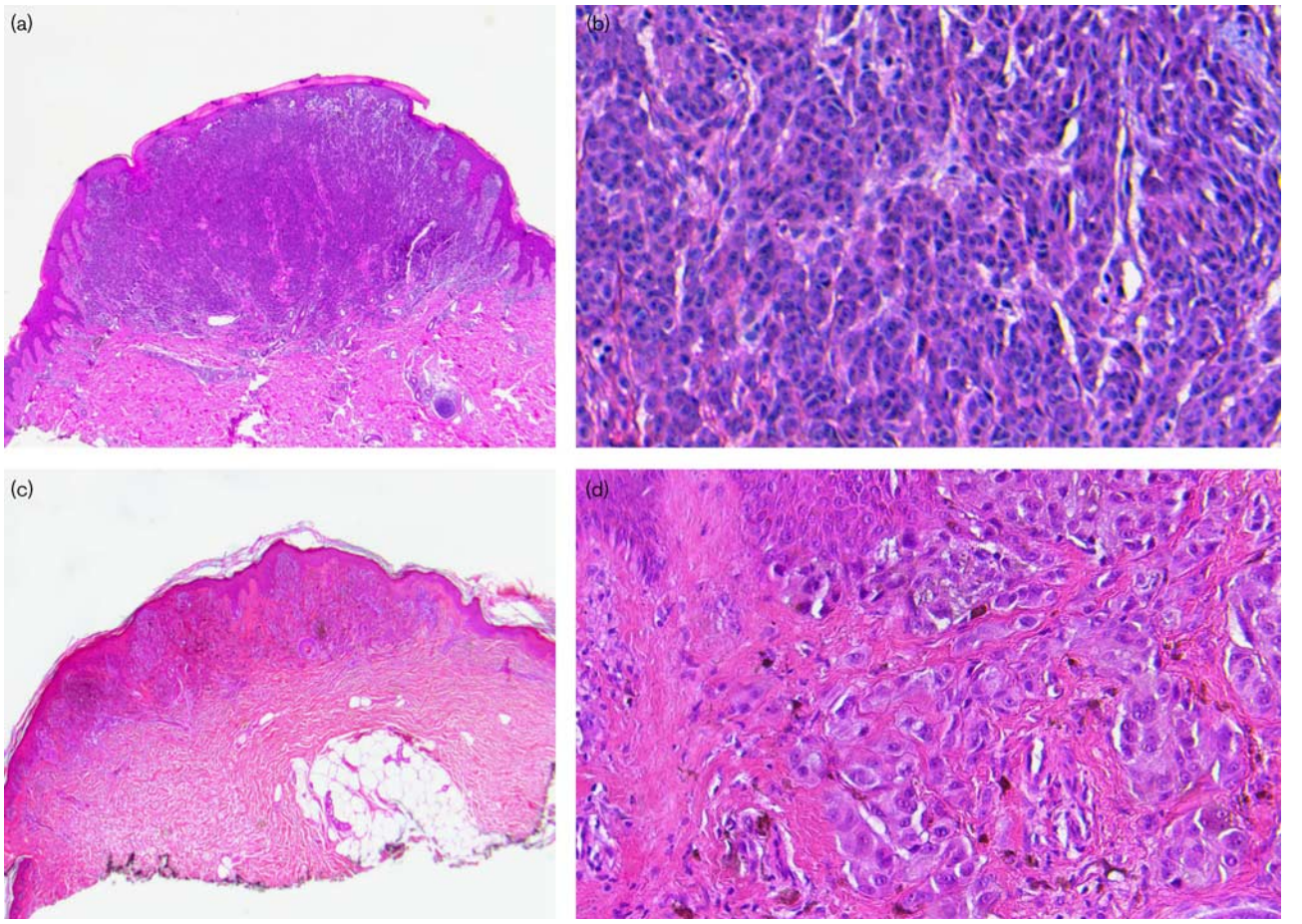

(a) Histology of a compound nevocellular nevi (NCN) used in this study. The dome-shaped lesion has a symmetrical composition and consists of junctional epidermal and dermal nevoid melanocytes. The epidermis shows hyperplasia with hyperkeratosis and parakeratosis and elongated rete ridges. There is only little dermal stroma in between the nevoid melanocytes. Hematoxylin–Eosin (H&E) staining, × 2.5 microscopic magnification factor. (b) Higher magnification from (a) showing nevoid melanocytes with an inconspicuous small nuclear size in relation to cytoplasmatic volume, indicating melanocyte maturation toward the depth of the lesion. There are no features of atypical morphology in the lesion, that is, asymmetry, mitotic figures, cytonuclear atypia, loss of maturation. H&E staining, × 20 microscopic magnification factor. (c) Histological morphology of a compound Spitz nevi (SN) from the SN cohort. The lesion has a symmetrical architecture with sharp lateral demarcation and a vague circumscription toward the depth. There is epidermal hyperplasia with hyperkeratosis and elongated rete ridges. Note the presence of prominent dermal collagenous, elastic, and vascular stroma in between the spitzoid melanocytes. H&E staining, × 2.5 microscopic magnification factor. (d) Higher magnification depicted from (c) showing a mixture of the characteristic epithelioid spitzoid melanocytic cells with abundant eosinophilic ground-glass cytoplasm containing vesicular nuclei with prominent nucleoli as well as a few spindle-shaped spitzoid melanocytes. Around the nevoid cell nests, retraction clefts are seen in relation to the surrounding prominent eosinophilic stroma. There is some stromal extra-melanocytic pigment deposition. H&E staining, × 20 microscopic magnification factor.

explore the molecular differences in 15 NCN compared with 25 SN. To minimize interindividual differences, we first studied gene expression in a training group consisting of seven patients in whom both a NCN and a SN were removed. Subsequently, the resulting differential gene profile was validated on a series of eight NCN and 18 SN.

Patients and methods

Patients and tissues

Formalin-fixed and paraffin-embedded (FFPE) excision specimens of patients harboring a SN, a NCN, or both were retrieved from the archives of the Department of Pathology at the University of Leuven, KUL Belgium, and the Maastricht Pathology Tissue Collection from the Department of Pathology, Maastricht University Medical Center, MUMC+, the Netherlands. All respective samples had been excised for diagnostic and therapeutic reasons. All use of tissue and patient data was in agreement with the Dutch Code of Conduct for Observational Research with Personal Data (2004) and Tissue (2001, *www.fmwv.nl*) with written informed consent from all participants in accordance with the Declaration of Helsinki. Diagnoses were defined previously by histology in routine diagnostics and were confirmed by three experienced dermatopathologists (V.W., J.VdO., L.M.H.). A total of 40 cases were included in the analysis. Of these, 15 were NCN (Fig. 1a and b) and 25

were histologically diagnosed as SN (Fig. 1c and d). In seven patients, both an NCN and an SN were available for study and represented the training set. SN were defined as benign melanocytic nevi composed of large epithelioid, oval, or spindled melanocytes arranged in nests and/or fascicles without significant cytonuclear atypia (Fig. 1c and d). The study was approved by the Maastricht Ethic Committee of the University of Maastricht, the Netherlands and by the Institutional Review Board of the University Hospitals of Leuven, Belgium (project number S 59659, 14 Februrary 2017).

Patient cohort

The training group consisted of seven patients with five women and two men ranging in age between 18 and 46 years (mean: 29.14 years, median: 26 years, Table 1). The lesions were localized on the extremities or on the corpus. No lesions were derived from the head and neck region. Histologically, one SN was diagnosed as dermal, two SN as junctional, and five as compound lesions. One compound SN (SN3) showed discrete dysplastic features with mild cytonuclear atypia and variation in cellular morphology, but did not fulfill the criteria for the diagnosis of an AST or STUMP. The same accounted for the patient's NCN (NCN3) with some degree of histological atypia, but not fulfilling the criteria for a dysplastic nevus. From all patients, the NCN and SN were removed at the same age, with the exception of patient number 7, with excision of his SN at the age of 18, followed by an excision of his NCN at the age of 24 years.

Table 1 Patient cohort with clinical data and histological diagnosis

Number of tissue specimens	Age	Sex	Tissue site	Histological features
Training set				
SN1	33	F	Upper leg	Dermal SN
NCN1	33	F	Upper leg	Dermal NCN
SN2	46	F	Upper leg	Compound SN
NCN2	46	F	Chest	Compound NCN
SN3	23	F	Abdomen	Compound SN with atypical features
NCN3	23	F	Back	Compound NCN with mild dysplasia
SN4	26	F	Upper leg	Junctional SN
NCN4	26	F	Axilla	Dermal NCN
SN5	31	M	Leg	Junctional SN
NCN5	31	M	Back	Compound NCN
SN6	24	F	Gluteal	Compound SN with angiomatous features
NCN6	24	F	Back	Compound NCN
SN7	18	M	Leg	Compound SN
NCN7	24	M	Upper arm	Compound NCN
Validation set NCN				
NCN8	42	F	Back	Dermal NCN
NCN9	19	F	Temporal	Dermal papillomatous NCN
NCN11	42	F	Upper leg	Dermal NCN
NCN12	45	M	Lumbar	Compound NCN with dysplastic features
NCN13	39	F	Abdomen	Dermal NCN
NCN14	33	M	Back	Junctional NCN
NCN15	26	M	Abdomen	Dermal NCN
NCN16	21	F	Back	Dermal NCN
Validation set SN				
SN8	58	F	Abdomen	Junctional SN
SN9	58	M	Unknown	Junctional SN
SN10	20	F	Upper leg	Junctional SN
SN11	35	F	Back	Compound SN
SN12	39	F	Cervical	Compound SN
SN14	44	M	Back	Compound SN
SN15	49	F	Knee	Compound SN
SN16	NA	NA	NA	Dermal SN
SN17	62	F	Arm	Dermal SN
SN18	42	F	Lower leg	Dermal SN
SN19	33	M	Unknown	Dermal SN
SN20	19	F	Arm	Dermal SN
SN21	24	M	Abdomen	Dermal SN
SN22	14	M	Lower leg	Compound SN
SN23	13	M	Lower arm	Dermal SN
SN24	32	F	Schoulder	Compound SN
SN25	14	M	Knee	Compound SN
SN26	29	F	Upper leg	Dermal SN

F, female; M, male; NA, not available; NCN, nevocellular nevus; SN, Spitz nevus.

The validation group consisted of 26 patients, with 15 female and 10 male patients showing a similar age distribution ranging from 13 to 62 years (mean: 34.08 years, median: 33 years, Table 1). From one patient, clinical data are not available (SN16). The NCN group consisted of 14 dermal, four junctional, and eight compound histological subtypes. Like the SN group, the NCN group showed localization on the extremities and the corpus, with the exception of NCN9, which had been excised from the temporal zone with a histological dermal papillomatous morphology, and SN12, which had been excised from the cervical area.

Tissue preparation and RNA isolation

Serial sections, 5 μm thick, were cut from FFPE tissue blocks using a microtome. One section per sample was mounted onto a glass slide and stained with Hematoxylin and Eosin, which served as the corresponding reference section to obtain at least 70% tumor purity. For RNA and DNA isolation, FFPE sections were collected in Eppendorf tubes, deparaffinized with xylol washing steps (1–4 times), and rehydrated in a graded alcohol series, starting at 100%, proceeding with 96%, and completing with 70% ethanol. Each time, tubes were washed with xylol/ethanol for 5 min in a centrifugation step for 5 min at 13000*g*. Subsequently, the pellets were dried for 1 h at 56°C. RNA and DNA were isolated using the AllPrep DNA/RNA FFPE kit (Qiagen, Hildesheim, Germany) according to the manufacturer's instructions. Purified RNA was measured in a spectrophotometer (Nanodrop, 2000; Thermo Scientific, Landsmeer, The Netherlands). Finally, another section was cut from the rest of the FFPE block and stained with Hematoxylin and Eosin, and the inclusion criteria were evaluated again on this section.

RNA expression analysis

mRNA expression was analyzed using the NanoString nCounter Gene Expression Platform (NanoString Technologies, Center of Medical Biotechnology, University Duisburg, Essen, Germany). The methodology detects the expression of up to 770 genes (including 40 housekeeping genes) from 13 canonical pathways including hallmark cancer genes (PanCancer Pathways Panel: *https://www.nanostring.com/products/gene-expression-panels/*

hallmarks-cancer-gene-expression-panel-collection/pancancer-pathways-panel). The mRNA array data are deposited in the NCBI's Gene Expression Omnibus database (accession number: GSE110589).

Bioinformatic and statistical analysis

The samples were dichotomized into a training set and a validation set. The training set included the seven NCN and the seven SN samples from the same seven patients to minimize interindividual genomic background. The second group of samples included eight NCN and 18 SN from different patients. All analyses were carried out using R-/Bioconductor (https://www.bioconductor.org/).

Positive and negative controls

Each assay included six positive and eight negative controls. A positive control normalization factor was calculated (with the geometric mean method). The negative controls were used to estimate the background (mean + 2SD). The average positive control normalization factor was low across assays, with 1.04 (range: 0.71–1.64). NanoString recommends a value between 0.3 and 3. The negative controls consistently produced a low value for the background (mean = 23.4; range: 6.68–40.97).

Marker discovery and validation

Testing for differential expression of the nCounter data in SN versus NCN was performed using the limma and the voom method in R [10]. The limma procedure has the advantage that it borrows information across all genes, which makes the analysis stable even when the sample size is small [11]. The voom procedure was used to nonparametrically estimate the mean–variance relationship of the log-transformed gene counts [12]. This procedure takes as input the raw counts and total library size (total number of counts) per sample is used as a scaling factor to normalize the counts. The voom procedure generates precision weights, which are incorporated into the limma linear modelling procedure and this removes the mean–variance relationship in the log-counts. The normalized log-counts were used in subsequent analyses.

The training set was first used to identify differentially expressed genes ($n = 14$; paired). All 770 genes were used as input for the analysis and adjusted for the paired study design, similar to a paired *t*-test. All significant genes ($P < 0.05$) were then further tested in the validation set ($n = 26$, red bars, Fig. 2c). Validated gene expression markers were those that were associated with SN versus NCN in the same direction in both datasets using a *P* value threshold of 0.05. False discovery rate (FDR) *q* values, adjusted for the tests that were performed in the validation dataset, were also calculated. A heatmap of the expression data was generated using pheatmap in R.

Building gene signatures

Gene signatures for SN versus NCN were generated using two statistical learning procedures: random forests (RF, Fig. 3a and b) and least absolute shrinkage and selection operator (LASSO, Fig. 3c and d) in R. To increase study power, all tissue samples were combined for these analyses (15 SN vs. 25 NCN). A gene classifier was generated using RF in R. The optimal value for the number of candidate gene expression variables that should be tried at every split was tuned ($n = 27$). To prevent overfitting, all the genes were used as input for the analyses. Five-hundred bootstrap samples were used. The out-of-bag (OOB) error was estimated, which is the average performance of the RF predictor using the samples not selected during bootstrap. The OOB error is therefore a valid estimate for the test error.

A LASSO signature was generated using glmnet in R. Five-fold cross-validation and the binomial deviance criterion were used to find the optimal tuning parameter for classification (lowest binomial deviance in cross-validation). Using this method, a model of gene expression markers was identified, where every marker had a corresponding LASSO coefficient, for distinguishing SN and NCN.

Gene set analysis

A pathway analysis was carried out using the camera method (limma in R) to identify sets of genes that are significantly upregulated or downregulated in SN compared with NCN [13]. A matrix of gene expression levels (number of genes = 770) in the different samples was used as input for the analysis. To increase power, the training and validation samples were combined similarly as described before for the RF and LASSO analyses. The following predefined Molecular Signatures Database (MSigDB) gene set categories were considered: Hallmark, Kegg, and Reactome. These gene sets were downloaded from *http://bioinf.wehi.edu.au/software/MSigDB/*.

Results

Differential gene expression in Spitz nevi versus nevocellular nevi

In the training set, 197 out of the 770 genes showed differential expression in the SN versus the NCN group ($P < 0.05$; Fig. 2a and Supplementary Fig. 1S, Supplemental digital content 1, *http://links.lww.com/MR/A62*). Seventy-five transcripts in the SN group had a higher mean expression level with a positive log-fold change (log FC) and 122 transcripts showed a lower mean expression level (negative log FC) compared with the NCN group. Of the 197 gene transcripts identified, 74 genes were validated in the second dataset ($P \leq 0.05$, FDR $q \leq 0.13$, Fig. 2b). Out of this set, 41 transcripts showed a positive log FC and 33 showed a negative log-FC. Figure 2c shows a heatmap of the 74 identified transcripts in all samples ($n = 40$). The gene transcript with the lowest log FC was *COL24A1* (log FC = −3.12). *PLA2G2A* showed the highest log FC (log FC = 2.80). The gene transcripts *COL24A1*, *FGF14*, *GZMB*, and *PLA2G2A* showed an absolute log FC of at least 2.

Fig. 2

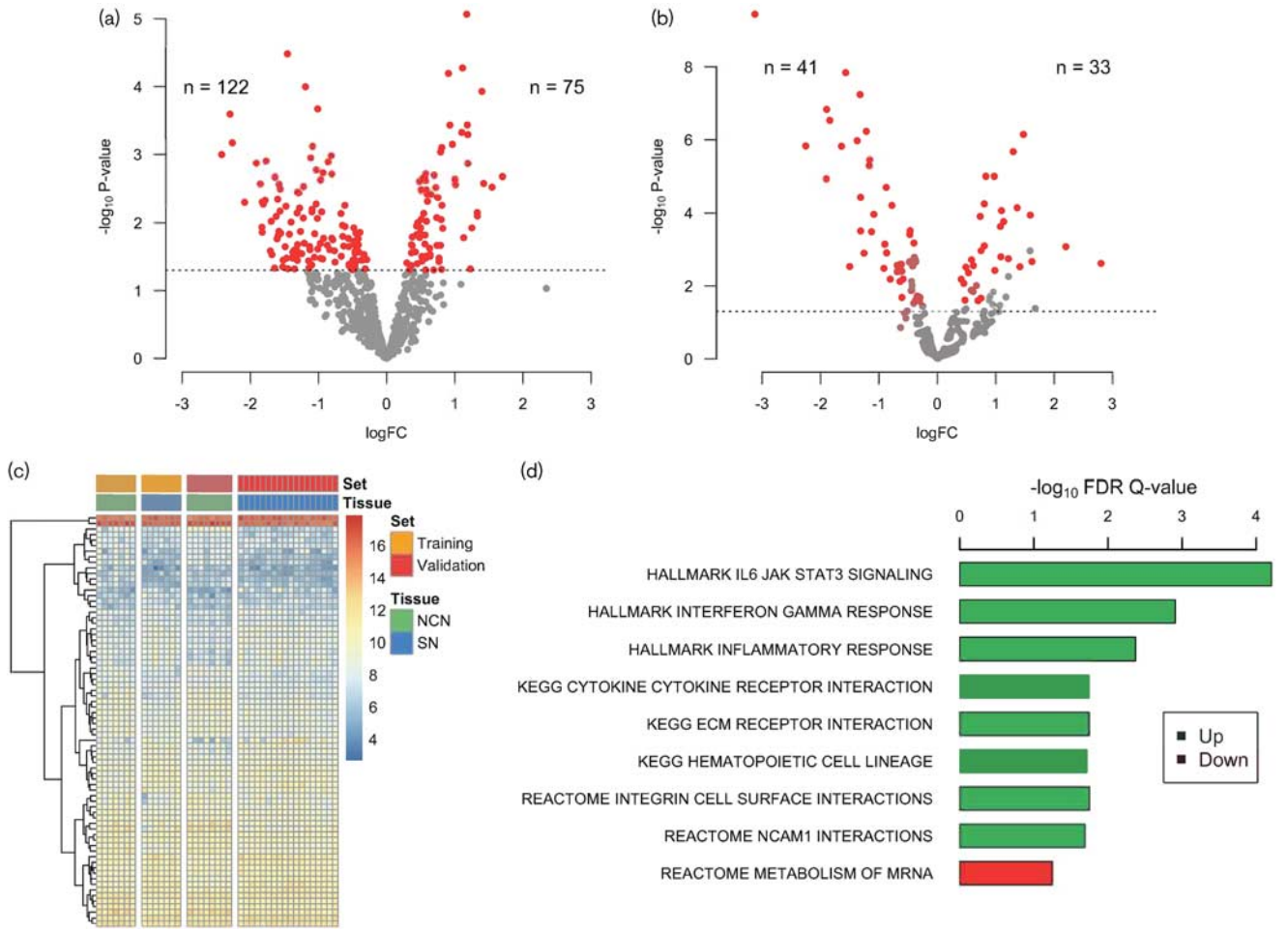

(a) Volcano plot identifying differentially expressed genes in Spitz nevi (SN) in relation to nevocellular nevi (NCN). In the training set, 197 genes were differentially expressed in SN versus NCN ($P < 0.05$), of which 75 had a higher mean expression level in SN (positive log-fold change, log FC) and 122 genes had a lower mean expression level in SN (negative log FC). Each dot represents a gene, and significant genes are shown in red. (b) Of the 197 genes identified in the training set, 74 were also differentially expressed in SN versus NCN in the validation set ($P < 0.05$, and same direction association; false discovery rate (FDR) $q \leq 0.13$). (c) A heatmap (supervised) of the 74 validated genes (rows) is shown for all 40 samples (columns). It shows that the 15 NCN (green bar) have a markedly different expression profile compared with the 25 SN (blue bar). The samples marked with an orange-colored bar represent the training set, whereas the samples marked with a red bar represent the validation set. The rows are clustered on the basis of the Euclidean distance and the complete linkage method. (d) The identified top-three ranked gene sets are listed, which were extracted from the Molecular Signature Databases (MSigDB). Results of the gene set analysis from Hallmark (50 gene sets), Kegg (129 gene sets), and Reactome (498 gene sets) are shown. Green bars show upregulation and the red bar shows downregulation of the gene set pathways.

Table 2 presents an overview of the discovered gene transcripts with log FC and *P* value for the discovery, that is, training set, and for the validation set as well as the FDR *q* value for each identified gene.

Pathway analysis

A Gene Set Enrichment Analysis was carried out to identify upregulated and downregulated pathways in SN compared with NCN using the camera method. Out of the 677 investigated MSigDB gene sets from Hallmark, KEGG, and Reactome, a top of nine gene pathways was identified. The MSigDB gene sets are included in the following broad categories: (i) cell cycle/proliferation; (ii) cytokine/immune/inflammatory; (iii) matrix/adhesion; (iv) hormone/receptor/signal transduction; and (v) transport and other. Figure 2d shows each of the top-three identified Hallmark, KEGG, and Reactome gene sets. All gene pathways were upregulated in SN compared with NCN, with the exception of the Reactome metabolism of the mRNA pathway. We found that four out of the top-ranked nine gene sets (all the Hallmark gene sets and the KEGG hematopoietic cell lineage gene pathway) were related to immunomodulatory and inflammatory processes. Three out of the nine gene sets showed involvement of ECM processes and interactions (two Reactome pathways and one Kegg pathway; see also

Fig. 3

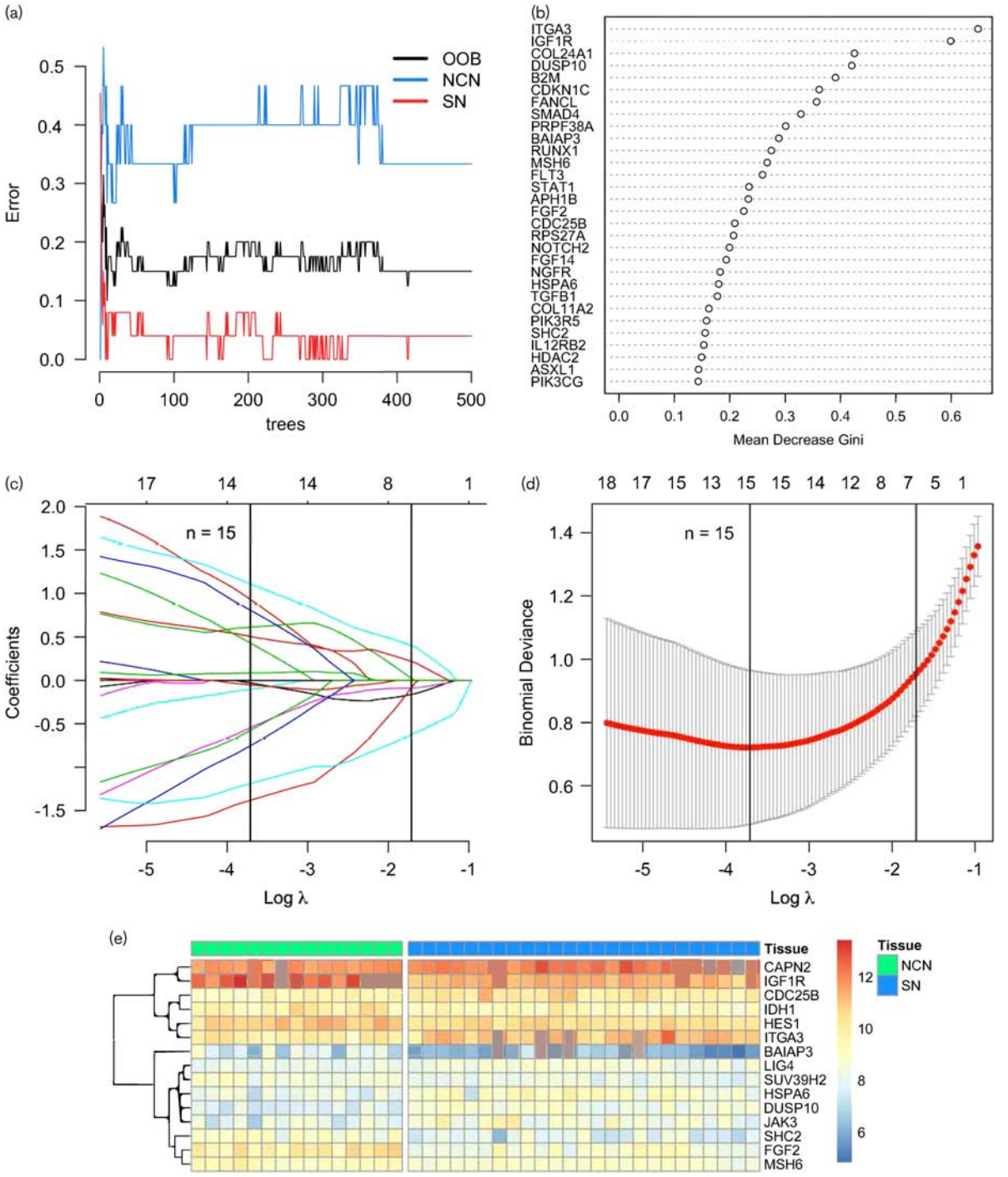

(a) The random forests (RF) procedure was used to build a multigene classifier with a Spitz nevi (SN) signature using expression data of 770 genes. The out-of-bag (OOB) estimate of the error rate was 15% (black line). The blue line shows the misclassification rate for the nevocellular nevi (NCN) group and the red line shows the misclassification rate for the SN group. (b) Variable importance of individual genes (*y*-axis) in the RF classifier as measured using the Gini impurity criterion. Mean Gini decrease rate is shown on the *x*-axis. (c) Coefficient path from LASSO regularization for classifying SN versus NCN. The colored lines represent individual genes and the *y*-axis shows the value of the coefficient associated with each marker, which is a function of log λ. The left-most vertical line shows the optimal log λ for classification, identified from five-fold cross-validation, which resulted in a sparse model that included 15 gene expression markers. The right-most vertical line represents the most regularized model such that error is within one standard error of the minimum (i.e. error of the 15-gene model). (d) The lowest binomial deviance from five-fold cross-validation is shown (left-most vertical line), and the corresponding log λ was chosen for variable selection as explained in (c). (e) Supervised heatmap of the 15 validated differentially expressed gene transcripts included in the signature. The samples are grouped by patients harboring a SN (blue colored bar) versus patients with an NCN (green colored bar). The rows of the heatmap represent the identified signature gens and each column is a patient sample of the NCN and SN group. The highest expression levels are shown in red staining and the lowest expression levels are shown in blue staining; yellow color represents intermediate expression (figure legend). The rows were clustered on the basis of the Euclidean distance and the complete linkage method.

Supplemental Table S1, Supplemental digital content 1, *http://links.lww.com/MR/A62*).

Identification of a molecular gene expression signature

Two different statistical learning methods (RF and LASSO) were used to create molecular profiles of the SN versus NCN group. For this analysis, the training and testing samples were combined. Using RF, a multigene classifier was created with an OOF error rate of 15% (Fig. 3a). The optimal value for the number of candidate gene expression variables that should be tried at every split was tuned ($n = 27$). The Gini impurity criterion was used to measure the importance of the individual genes obtained from the RF analysis (Fig. 3b). As such, the two top-ranked genes are *ITGA3* and *IGFR1*.

Then, the LASSO method was used. Five-fold cross-validation identified the value for the tuning parameter that resulted in the lowest binomial deviance for classification (Fig. 3c and d). From the analysis, a molecular signature consisting of 15 top-ranked differentially expressed gene transcripts was derived. Figure 3e shows a supervised heatmap of the identified genes. *CAPN2*, *CDC25B*, *ITGA3*, *LIG4*, *HSPA6*, *DUSP10*, and *JAK3* were upregulated in the SN compared with the NCN group. *IGFR1*, *IDH1*, *HES1*, *BAIAP3*, *SUV39H2*, *SHC2*, *FGF2*, and *MSH6* transcripts showed lower expression in the SN group. Table 3 provides detailed information about the top-ranked differentially expressed gene transcripts. The identified gene transcripts showed genome-wide localization (including chromosomes 1, 2, 3, 4, 10, 13, 15, 16, 17, 19, 20). The distribution of the differentially expressed gene transcripts across the genome is highlighted in a Manhattan plot (Supplementary Fig. 2S, Supplemental digital content 1, *http://links.lww.com/MR/A62*).

It is noteworthy that four of the top-ranked signature genes identified with the LASSO and RF procedure (*JAK3*, *HES1*, *LIG*1, and *IDH1*, Table 3 and Fig. 3a–e) are not within the group of the 74 genes differentially expressed genes in SN versus NCN (Table 2 and Fig. 2–c). The reason for this different statistical outcome is that the LASSO and RF analysis uses all samples in a single cohort. In contrast, the total group of samples is divided into a paired training set and validated in a validation set in the differential expression analysis using limma. In the differential expression analysis, the *P* value for those four genes is greater than 0.05 either in the training set or in the validation set. The *P* value for *HES1*, *LIG4*, and *IDH1* exceeds 0.05 in the training group (0.07, 0.08, and 0.41, respectively). For *JAK3*, the *P* value is 0.09 in the validatiom group. Increasing the number of samples in the combined analysis yields statistically significant results.

Discussion

In the present study, we have identified and validated which genes are differentially expressed in SN compared with NCN using NanoString nCounter expression profiling with a probe set of 770 genes related to cancer, growth, and invasion. To minimize interindividual differences, we studied expression levels of both types of nevi within the same individuals and validated the results in a larger group of lesions. Following this approach, we could identify a molecular signature that can distinguish SN from NCN. Our findings strongly indicate that spitzoid melanocytic lesions represent a distinct subgroup of melanocytic neoplasms [9,14]. Many molecular studies have been carried out on the various types of spitzoid lesions, but the basic molecular characteristics of benign spitzoid lesions and their differences from common NCN are known to a lesser degree [15]. Therefore, the aim of this study was to identify a discriminating expression profile of SN in relation to NCN and define a list of genes that may be able to provide new insights into this gap in knowledge from a molecular standpoint.

The expression profile of SN in comparison with NCN was investigated using NanoString nCounter expression profiling, which is based on the detection of RNA expression differences. This platform has been used to identify RNA expression patterns to accurately diagnose and classify different tumor types and grades including pancreatic, breast, and colorectal cancer [16–18]. We applied customized NanoString expression analysis using the PanCancer pathway panel, which does not require reverse transcription or amplification. The measurement of gene expression at the RNA level yields information on the actual functional state of a cell. However, as mRNA levels do not necessarily reflect protein expression, we are currently investigating the identified signature genes on the protein level using immunohistochemistry staining.

The limma software package was used to test for differential expression in the SN group versus the NCN group [10]. An important feature of limma is that it borrows information across genes, which makes it powerful even when the total sample size is small [11]. Our results showed distinct expression profiles for SN and NCN that resulted in the separation of cases into two clusters. We could clearly differentiate NCN from SN in the validation cohort when the discriminatory criteria obtained from the training cohort were used. Two different learning methods (RF and LASSO) were used to identify the molecular signature of SN in relation to NCN. Different from the RF method, the LASSO method performs model fitting and variable selection. The method was used to generate a model of important genes that optimally distinguishes SN from NCN samples.

In the training set, 122 genes showed a negative log FC and 75 genes showed a positive log FC. Out of this set, 41 transcripts validated with a positive log FC and 33 showed a negative log FC (Fig. 2a and b). The reason why many downregulated genes did not validate in the final analysis might be skipping of gene filtering before the analysis. Gene filtering was not applied to prevent

Table 2 Identified 74 differentially expressed genes in Spitz nevi versus nevocellular nevi

Genes	Log FC training set	*P* training set	Log FC validation set	*P* validation set	FDR *q* validation set
COL24A1	−0.76	3.80E−02	−3.12	3.63E−10	7.15E−08
FGF2	−1.02	8.60E−03	−1.57	1.45E−08	1.42E−06
IGF1R	−1.11	1.13E−03	−1.32	5.72E−08	3.76E−06
BAIAP3	−1.64	2.13E−03	−1.90	1.47E−07	7.26E−06
COL27A1	−0.61	1.13E−02	−1.84	2.98E−07	1.17E−05
APH1B	−0.67	7.29E−03	−1.22	5.98E−07	1.96E−05
PIK3R5	0.63	2.37E−02	1.48	7.19E−07	2.02E−05
FANCL	−0.87	2.13E−02	−1.37	1.06E−06	2.62E−05
GNG7	−1.22	8.49E−03	−1.64	1.51E−06	2.97E−05
FGF14	−2.27	6.75E−04	−2.25	1.48E−06	2.97E−05
ITGA3	1.19	3.67E−04	1.30	2.16E−06	3.87E−05
PDGFD	−0.55	4.32E−02	−1.16	3.59E−06	5.89E−05
SHC2	−1.19	1.01E−04	−1.17	5.17E−06	7.84E−05
COL5A2	0.56	2.05E−02	0.98	1.00E−05	1.34E−04
MYD88	0.54	7.25E−03	0.83	1.02E−05	1.34E−04
PAX3	−0.97	2.02E−02	−1.90	1.17E−05	1.44E−04
RPS27A	−0.48	1.19E−02	−0.88	2.00E−05	2.32E−04
COL11A2	−1.56	3.20E−03	−1.32	3.69E−05	4.04E−04
DUSP10	1.11	4.74E−04	0.81	5.65E−05	5.86E−04
MET	−0.49	1.89E−02	−0.78	6.11E−05	6.02E−04
STAT1	1.19	5.09E−04	1.36	7.18E−05	6.73E−04
PIK3CG	0.64	2.92E−02	1.10	8.55E−05	7.66E−04
RNF43	−0.63	2.20E−02	−1.08	1.08E−04	9.28E−04
IL2RB	1.43	2.64E−03	1.59	1.14E−04	9.37E−04
B2M	0.65	3.80E−03	0.73	1.22E−04	9.62E−04
FLT3	1.33	7.95E−03	1.14	1.70E−04	1.29E−03
RUNX1	0.93	3.69E−04	1.08	2.33E−04	1.70E−03
MSH6	−0.47	4.47E−02	−0.47	3.04E−04	2.11E−03
CASP12	−1.91	1.34E−03	−1.31	3.10E−04	2.11E−03
CDKN1C	−1.46	3.27E−05	−1.13	3.24E−04	2.13E−03
AKT2	−0.42	1.71E−02	−0.47	3.85E−04	2.45E−03
SMAD4	−0.41	2.11E−02	−0.40	6.62E−04	4.08E−03
BAMBI	−0.94	3.41E−02	−0.90	7.15E−04	4.27E−03
HSPA6	0.81	7.91E−04	0.80	7.93E−04	4.60E−03
GZMB	1.70	2.11E−03	2.20	8.38E−04	4.72E−03
HHEX	0.45	4.01E−02	0.75	1.07E−03	5.85E−03
ARNT2	−0.84	2.49E−02	−0.87	1.24E−03	6.53E−03
BIRC7	−1.31	7.17E−03	−1.26	1.26E−03	6.53E−03
RAC2	1.01	2.75E−03	1.09	1.58E−03	8.00E−03
NGFR	0.79	9.18E−04	1.21	1.79E−03	8.82E−03
TGFB1	0.91	6.42E−05	0.58	1.93E−03	9.26E−03
MMP9	1.00	2.31E−03	1.62	2.13E−03	9.98E−03
BRAF	−0.81	1.04E−03	−0.48	2.19E−03	1.00E−02
PLA2G2A	1.55	2.98E−03	2.80	2.38E−03	1.06E−02
AKT3	−0.86	1.29E−03	−0.62	2.54E−03	1.11E−02
SYK	0.58	3.26E−03	0.62	2.77E−03	1.18E−02
SUV39H2	−0.56	1.70E−02	−0.42	2.81E−03	1.18E−02
IL7R	0.81	4.85E−02	1.41	2.96E−03	1.19E−02
PLA1A	−1.53	4.45E−02	−1.50	2.94E−03	1.19E−02
CAPN2	0.36	4.25E−02	0.49	3.05E−03	1.20E−02
PPP2R2B	−1.29	3.62E−03	−0.92	3.29E−03	1.27E−02
THBS1	0.79	2.15E−02	0.98	3.71E−03	1.41E−02
EPOR	−0.81	1.68E−02	−0.61	3.92E−03	1.46E−02
RAC3	−0.55	4.08E−02	−0.68	4.02E−03	1.47E−02
PLCG2	0.75	4.24E−03	0.53	4.34E−03	1.55E−02
TGFBR2	0.44	1.11E−02	0.41	6.54E−03	2.23E−02
IL20RA	−0.50	4.92E−02	−0.59	6.42E−03	2.23E−02
CDKN2A	−0.79	1.78E−02	−0.81	6.57E−03	2.23E−02
HDAC11	−0.93	1.86E−03	−0.64	7.49E−03	2.50E−02
CDC25B	1.18	8.59E−06	0.45	8.47E−03	2.78E−02
IL1R1	0.96	7.09E−04	0.58	1.31E−02	4.15E−02
ALKBH2	−0.56	2.24E−02	−0.44	1.30E−02	4.15E−02
COL4A4	0.77	3.38E−02	0.61	1.42E−02	4.45E−02
ARID1B	−0.39	1.39E−02	−0.30	2.06E−02	6.27E−02
FZD9	−1.22	2.92E−03	−0.61	2.07E−02	6.27E−02
TNF	0.74	2.15E−02	0.75	2.19E−02	6.53E−02
CASP8	0.57	1.91E−03	0.47	2.45E−02	7.14E−02
GNG12	−0.80	1.94E−03	−0.38	2.47E−02	7.14E−02
INHBA	1.13	1.66E−02	0.70	2.57E−02	7.33E−02
XPA	−0.44	1.80E−02	−0.30	2.67E−02	7.53E−02
KMT2D	−0.35	3.52E−02	−0.25	3.62E−02	1.00E−01
CSF1R	0.57	3.30E−02	0.49	4.24E−02	1.16E−01
TNFSF10	0.59	3.78E−03	0.46	4.70E−02	1.27E−01
TSPAN7	−1.03	1.69E−03	−0.51	4.87E−02	1.30E−01

FDR, false discovery rate; log FC, log-fold change; *P*, *P* value.

Table 3 Characteristics of 15 top-ranked differentially expressed genes in Spitz nevi versus nevocellular nevi

Genes	Chromosome	Reference sequence ID	Protein description	Subcellular localization of protein	Function	Gene to cellular pathway mapping	*P* value training set	*P* value validation set
CAPN2: Calpain-2 catalytic subunit	1	NM_001748.4	Calcium-activated cysteine protease	Cytoplasm	Cell growth, cytoskeletal rearrangement	Apoptosis	0.0425	0.0030
IGF1R: Insulin-like growth factor 1 receptor	15	NM_000875.2	Tyrosine kinase receptor	Membrane	Cell growth	PI3K, RAS	0.0011	0.0000
CDC25B: Homo sapiens cell division cycle 25A	20	NM_021873.2	Phosphatase	Nucleus and cytoplasm	Cell growth	MAPK, apoptosis	0.0000	0.0085
IDH1: Isocitrate dehydrogenase 1 (NADP+), soluble	2	NM_005896.2	Isocitrate dehydrogenase 1	Cytoplasm	Glucose metabolism	Driver gene	0.4131	0.0004
HES1: Hairy and enhancer of split−1	3	NM_005524.2	Transcription factor	Nucleus	Cell growth	Notch	0.0704	0.0000
ITGA3: Integrin α 3	17	NM_005501.2	ECM protein	Membrane	Intercellular interaction	PI3K	0.0004	0.0000
BAIAP3: Brain angiogenesis inhibitor associated protein 3	16	NM_003933.4	Secretin receptor family	Membrane	Intercellular interaction, regulation of synaptic functions	MAPK	0.0021	0.0000
LIG4: DNA ligase 4	13	NM_002312.3	DNA ligase	Nucleus	DNA repair	DNA repair	0.0792	0.0478
SUV39H2: Suppressor of variegation 3–9 homolog 2	10	NM_024670.3	Methyltransferase	Nucleus	Chromatin modification	DNA repair	0.0170	0.0028
HSPA6: Heat-shock protein 6	1	NM_002155.3	Chaperone	Nucleus and cytoplasm	mRNA splicing, proteolysis	MAPK	0.0008	0.0008
DUSP10: Dual specificity protein phosphatases 10	1	NM_144728.2	Phosphatase	Nucleus and cytoplasm	Inactivates p38 and SAPK/JNK in the MAPK/ERK, SAPK/JNK/p38 pathway	MAPK	0.0005	0.0001
JAK3: Janus kinase 3	19	NM_000215.2	Janus kinase	Nucleus and cytoplasm	Signal downstream in RAS–RAF–MAPK and PI3K pathway	Driver gene	0.0014	0.0920
SHC2: Src homology 2 domain containing transforming protein 2	19	NM_012435.2	Phosphoprotein receptor tyrosine kinase binding	Cytoplasm and membrane	Cell growth	RAS	0.0001	0.0000
FGF2: Fibroblast growth factor 2, basic	4	NM_002006.4	Growth factor protein	Extracellular/secreted, cytoplasm and nucleus	Cell growth, differentiation, angiogenesis	MAPK, PI3K, RAS	0.0086	0.0000
MSH6: MutS homolog 6	2	NM_000179.1	DNA mismatch repair protein	Nucleus	Nucleotide binding, belongs to the postreplicative DNA mismatch repair system	Driver gene	0.0447	0.0003

ECM, extracellular matrix; ID, identification; MAPK, mitogen-activated protein kinase; PI3K, phosphoinositide 3-kinase.

any form of selection bias to the subsequent analytical steps. Furthermore, many NCN in the training set showed a positive normalization factor and a relatively small library size with a lower RNA content. Although the samples were adjusted for this, it cannot be ruled out that very low expression levels might actually represent missing information. However, there should not be too much concern about this finding because gene discovery analysis with high-dimensional data usually leads to the discovery of many false positives. It should also be noted that we did not adjust for multiple testing in the training set, but used a *P* value less than 0.05 as criterion. Most importantly, we validated the data on a larger validation set and could remove many false positives immediately.

Gene set enrichment analysis showed that the molecular profile of SN was related to inflammatory/immunomodulatory processes and ECM interactions as well as angiogenesis-related processes. This is in line with histological observations; many SN are characterized by infiltration of lymphocytes and their stroma may show pronounced desmoplasia and increased numbers of capillaries and postcapillary venules [3,19,20]. In the group of the 74 differentially expressed genes (Table 2), there was upregulation of *GZMB* (Granzyme B) in the SN group versus the NCN group, with a positive log FC of 2.2 (validation group) and log FC of 1.7 (training group). As assumed earlier in the literature, the reason might be an increased T-cell-bound CD8+ cytotoxic immune response in SN compared with NCN [21].

The identified gene transcripts of the SN signature comprise transcription factors (e.g. *HES1*) regulating cell division and growth, DNA repair molecules (e.g. *MSH6*, *LIG4*, *SUV39H2*), mRNA splicing proteins (e.g. *HSPA6*), tyrosine kinase receptores (e.g. *IGFR1*), kinases (e.g. *JAK3*), phosphatases (e.g. *SHC2*, *DUSP10*, *CDC25B*), proteases (e.g. *CAPN2*), cell adhesion, and ECM-associated molecules (e.g. *ITGA3*, *FGF2*) as well as transcripts associated with angiogenesis-associated processes (e.g. *BAIAP3*). Furthermore, downregulation of isocitrate dehydrogenase 1 (*IDH1*) was identified in the SN signature (log FC: −0.133). Previously, mutations in *IDH1* have been detected in an integrated genomic analysis of human glioblastoma multiforme [22]. *IDH1* alterations often represent the first hit in the development of diffuse gliomas. Recently, Lazova *et al.* [15] detected upregulation of *IDH1* in an exome sequencing study in their spitzoid melanoma samples, their conventional melanoma samples, and in one of their common nevi. However, they did not detect upregulated expression of *IDH1* in their SN group, which is line with our current findings. Hence, one may speculate that *IDH1* immunohistochemistry staining might be a promising tool in the differential diagnosis between various spitzoid neoplasms.

In our study, the SN group showed lower expression of insulin-like growth factor 1 receptor (*IGF1R*, log FC = −1.32) compared with the NCN group. *IGF1R* functions as a transmembrane tyrosine kinase receptor and is activiated by its related hormones insulin-like growth factors 1 and 2 (*IGF-1* and *IGF-2*). *IGF* represents a polypeptide hormone similar in molecular structure to insulin and plays an important role in cell growth. Upregulation of *IGF1R* has been described in several human malignancies [23,24] as well as cutaneous melanomas [25]. Overexpression of the *IGF-1R* has been reported in relation to resistance development toward the BRAF V600 inhibitor vemurafenib [26–28]. Currently, we lack an explanation for this paradox of the upregulated expression of IGF1R in the NCN group versus the SN group.

The presented data show a differential expression of mRNA transcripts in the SN group compared with the NCN group. Currently, we are validating the identified top-ranked gene transcripts of SN with immunohistochemistry staining to find out whether the signature is also discriminative at the protein level. We also aim to validate this signature by NanoString nCounter gene expression analysis in a larger group of SN and NCN that were in the original list of cases. Finally, we aim to find out in the future whether the identified SN signature shows consistent changes in AST/STUMP and in SMM, and thus, whether it can contribute toward diagnosis in daily surgical pathology practice.

Conclusion

This is the first study using NanoString nCounter Data as a novel tool in the evaluation of Spitzoid neoplasms. We identified significantly differentially expressed genes in SN compared with NCN even when analyzing the same individuals. These findings support the hypothesis that SN most likely constitute a distinct neoplastic melanocytic group that is different from other melanocytic neoplasms. The identification of the basic molecular differences in benign Spitzoid lesions may be useful in the future to develop optimal criteria for the differential diagnosis of SN from AST/STUMP and SMM.

Acknowledgements

This work was supported financially by the academic incentive fund from the Maastricht University Hospital Center, MUMC+, the Netherlands.

Conflicts of interest

There are no conflicts of interest.

References

1 Requena C, Requena L, Kutzner H, Sánchez Yus E. Spitz nevus: a clinicopathological study of 349 cases. *Am J Dermatopathol* 2009; **31**:107–116.
2 Spitz S. Melanomas of childhood. *Am J Pathol* 1948; **24**:591–609.
3 Weedon D, Little JH. The Spitz naevus. *Aust N Z J Surg* 1978; **48**:21–22.
4 Lallas A, Kyrgidis A, Ferrara G, Kittler H, Apalla Z, Castagnetti F, *et al.* Atypical Spitz tumours and sentinel lymph node biopsy: a systematic review. *Lancet Oncol* 2014; **15**:178–183.

5 Cerroni L, Barnhill R, Elder D, Gottlieb G, Heenan P, Kutzner H, *et al*. Melanocytic tumors of uncertain malignant potential: results of a tutorial held at the XXIX Symposium of the International Society of Dermatopathology in Graz, October 2008. *Am J Surg Pathol* 2010; **34**:314–326.

6 McCormack CJ, Conyers RK, Scolyer RA, Kirkwood J, Speakman D, Wong N, *et al*. Atypical Spitzoid neoplasms: a review of potential markers of biological behavior including sentinel node biopsy. *Melanoma Res* 2014; **24**:437–447.

7 Bradish JR, Cheng L. Molecular pathology of malignant melanoma: changing the clinical practice paradigm toward a personalized approach. *Hum Pathol* 2014; **45**:1315–1326.

8 Cancer Genome Atlas Network. Genomic classification of cutaneous melanoma. *Cell* 2015; **161**:1681–1696.

9 Wiesner T, He J, Yelensky R, Esteve-Puig R, Botton T, Yeh I, *et al*. Kinase fusions are frequent in Spitz tumours and spitzoid melanomas. *Nat Commun* 2014; **5**:3116.

10 Green R, Wilkins C, Thomas S, Sekine A, Ireton RC, Ferris MT, *et al*. Identifying protective host gene expression signatures within the spleen during West Nile virus infection in the collaborative cross model. *Genom Data* 2016; **10**:114–117.

11 Ritchie ME, Phipson B, Wu D, Hu Y, Law CW, Shi W, *et al*. limma powers differential expression analyses for RNA-sequencing and microarray studies. *Nucleic Acids Res* 2015; **43**:47.

12 Law CW, Chen Y, Shi W, Smyth GK. voom: Precision weights unlock linear model analysis tools for RNA-seq read counts. *Genome Biol* 2014; **15**:29.

13 Wu D, Smyth GK. Camera: a competitive gene set test accounting for inter-gene correlation. *Nucleic Acids Res* 2012; **40**:133.

14 Bastian BC. The molecular pathology of melanoma: an integrated taxonomy of melanocytic neoplasia. *Annu Rev Pathol* 2014; **9**:239–271.

15 Lazova R, Pornputtapong N, Halaban R, Bosenberg M, Bai Y, Chai H, *et al*. Spitz nevi and Spitzoid melanomas: exome sequencing and comparison with conventional melanocytic nevi and melanomas. *Mod Pathol* 2017; **30**:640–649.

16 Garcia PL, Miller AL, Kreitzburg KM, Council LN, Gamblin TL, Christein JD, *et al*. The BET bromodomain inhibitor JQ1 suppresses growth of pancreatic ductal adenocarcinoma in patient-derived xenograft models. *Oncogene* 2016; **35**:833–845.

17 Brasó-Maristany F, Filosto S, Catchpole S, Marlow R, Quist J, Francesch-Domenech E, *et al*. PIM1 kinase regulates cell death, tumor growth and chemotherapy response in triple-negative breast cancer. *Nat Med* 2016; **22**:1303–1313.

18 Suzuki Y, Ng SB, Chua C, Leow WQ, Chng J, Liu SY, *et al*. Multiregion ultra-deep sequencing reveals early intermixing and variable levels of intratumoral heterogeneity in colorectal cancer. *Mol Oncol* 2017; **11**:124–139.

19 Weedon D, Little JH. Spindle and epithelioid cell nevi in children and adults. A review of 211 cases of the Spitz nevus. *Cancer* 1977; **40**:217–225.

20 Piepkorn M. On the nature of histologic observations: the case of the Spitz nevus. *J Am Acad Dermatol* 1995; **32** (**Pt 1**):248–254.

21 Birck A, thor Straten P, Li L, Hou-Jensen K, Sugár J, Zeuthen J. Analysis of T cell receptor AV and BV chain gene expression by infiltrating lymphocytes in Spitz naevi and in halo naevi. *Melanoma Res* 1997; **7**:49–57.

22 Parsons DW, Jones S, Zhang X, Lin JC, Leary RJ, Angenendt P, *et al*. An integrated genomic analysis of human glioblastoma multiforme. *Science* 2008; **321**:1807–1812.

23 Samani AA, Yakar S, LeRoith D, Brodt P. The role of the IGF system in cancer growth and metastasis: overview and recent insights. *Endocr Rev* 2007; **28**:20–47.

24 Werner H. Tumor suppressors govern insulin-like growth factor signaling pathways: implications in metabolism and cancer. *Oncogene* 2012; **31**:2703–2714.

25 Capoluongo E. Insulin-like growth factor system and sporadic malignant melanoma. *Am J Pathol* 2011; **178**:26–31.

26 Villanueva J, Vultur A, Lee JT, Somasundaram R, Fukunaga-Kalabis M, Cipolla AK, *et al*. Acquired resistance to BRAF inhibitors mediated by a RAF kinase switch in melanoma can be overcome by cotargeting MEK and IGF-1R/PI3K. *Cancer Cell* 2010; **18**:683–695.

27 Villanueva J, Vultur A, Herlyn M. Resistance to BRAF inhibitors: unraveling mechanisms and future treatment options. *Cancer Res* 2011; **71**:7137–7140.

28 Wang J, Sinnberg T, Niessner H, Dölker R, Sauer B, Kempf WE, *et al*. PTEN regulates IGF-1R-mediated therapy resistance in melanoma. *Pigment Cell Melanoma Res* 2015; **28**:572–589.